Supporting Information

Delvendahl et al. 10.1073/pnas.1508419112

SI Materials and Methods

Calibration of Two-Photon Ca^{2+} Imaging. To quantify the intracellular $[Ca^{2+}]$ with Ca^{2+} indicators of different affinity, minimum (R_{min}) and maximum (R_{max}) fluorescence ratios were determined in situ with 10 mM EGTA or 10 mM $CaCl_2$ in the intracellular solution. Fluorescence ratios for calibration were not significantly different in cMFBs and granule cells but were consistently about twofold higher than in pipettes (Fig. S1*A*). A discrepancy in calibration ratios between in-cell and pipette measurements is a well-known phenomenon with multiple reasons, such as accumulation of fluorophores in subcellular compartments (1, 2), increased intracellular fluorescence of Ca^{2+} indicators because of cytosolic viscosity (3), different bleaching behavior of fluorophores (4), or difficulty to clamp intracellular Ca^{2+} concentration (5). In our case, insufficient clamping of intracellular $[Ca^{2+}]$ is unlikely for two reasons. First, cMFBs are small and directly attached to the pipette via comparably low access resistance, resulting in rapid diffusional equilibration. Second, one might expect that R_{max} values differ more between cells and pipettes because of strong extrusion mechanisms (5). In contrast, we observed almost identical cell-to-pipette factors for R_{min} and R_{max} (Fig. S1*A*).

Determination of R_{min} can be difficult for low-affinity dyes, resulting in possible errors of Ca^{2+} amplitude estimation due to incorrect high values for $[Ca^{2+}]_{rest}$. However, deliberately adjusting R_{min} values of Fluo-4FF and OGB-5N so that $[Ca^{2+}]_{rest}$ = 57 nM (Fig. S1*B*) resulted in a reduction of Ca^{2+} amplitudes of, on average, less than 4%. Thus, the potential uncertainty in determining R_{min} for these dyes is unlikely to appreciably confound our results.

Single-Indicator Quantification. For experiments with OGB-1, we also used a single-indicator method (6) for calculation of $[Ca^{2+}]$

$$\left[Ca^{2+}\right] = K_D \frac{F/F_{max} - R_f^{-1}}{1 - F/F_{max}}, \qquad \textbf{[S1]}$$

where F denotes the fluorescence in the green channel, R_f is the dynamic range of the dye, and F_{max} the maximum fluorescence as determined during a train of 20 stimuli at 300 Hz in each experiment. R_f for the high-affinity dye OGB-1 was determined as 5.9 in our experiments (6). We calculated $[Ca^{2+}]_{rest}$ with Eq. **1** for the dual-indicator approach or by using the following equation for the single-indicator approach:

$$\left[Ca^{2+}\right]_{rest} = K_D \left[\frac{\left(1 - R_f^{-1}\right)}{F_{max}} - R_f^{-1}\right]. \qquad \textbf{[S2]}$$

Single- and dual-indicator methods gave very similar results (Figs. S1*B* and S3*A*).

Dissociation Constants of Ca^{2+} Indicators. For calculation of $\kappa_{E,fixed}$, AP-evoked amplitude, and time constant (Fig. 2), we compared three different sets of dissociation constants (K_D) for the four Ca^{2+}-sensitive dyes (OGB-5N, Fluo-4FF, Fluo-5F, and OGB-1):

i) Literature values determined for recording conditions at 34 °C: K_D = 32, 8.1, 1.3, and 0.21 μM, respectively (7, 8). Resulting parameters were $\kappa_{E,fixed}$ = 11 ± 8 and 17 ± 7 from A^{-1} and τ extrapolation, A = 0.31 μM [0.19–0.82 μM], and τ = 67 ± 24 ms.

ii) Cuvette values measured at room temperature (Fig. S2): K_D = 22.1, 15.3, 0.77, and 0.22 μM, respectively. Using these K_D values resulted in $\kappa_{E,fixed}$ = 18 ± 8 and 12 ± 8 from A^{-1} and τ extrapolation, respectively, A = 0.19 μM [0.14–0.31 μM], and τ = 45 ± 25 ms.

iii) Measured cuvette values scaled by a factor of 1.08: K_D = 24.0, 16.6, 0.83, and 0.24 μM, respectively. The scaling factor (1.08) was chosen to obtain a mean of the four K_D values identical to the mean of the four literature values. The resulting parameters were $\kappa_{E,fixed}$ = 17.5 ± 7.5 and 12.7 ± 7.2 from A^{-1} and τ extrapolation, respectively, A = 0.20 μM [0.15–0.32 μM], and τ = 50 ± 25 ms (Fig. 2 and Fig. S3).

Thus, the estimated parameters (e.g., $\kappa_{E,fixed}$) were very similar with these three sets of K_D values. We therefore used the latter set of K_D values throughout the manuscript.

1. Neher E, Augustine GJ (1992) Calcium gradients and buffers in bovine chromaffin cells. *J Physiol* 450:273–301.
2. Hernández-Cruz A, Sala F, Adams PR (1990) Subcellular calcium transients visualized by confocal microscopy in a voltage-clamped vertebrate neuron. *Science* 247(4944):858–862.
3. Poenie M (1990) Alteration of intracellular Fura-2 fluorescence by viscosity: A simple correction. *Cell Calcium* 11(2-3):85–91.
4. Benson DM, Bryan J, Plant AL, Gotto AM, Jr, Smith LC (1985) Digital imaging fluorescence microscopy: Spatial heterogeneity of photobleaching rate constants in individual cells. *J Cell Biol* 100(4):1309–1323.
5. Schneggenburger R (2005) Ca^{2+} uncaging in nerve terminals. *Imaging in Neuroscience and Development*, eds Yuste R, Konnerth A (Cold Spring Harbor Laboratory Press, Cold Spring Harbor, NY), pp 415–419.
6. Maravall M, Mainen ZF, Sabatini BL, Svoboda K (2000) Estimating intracellular calcium concentrations and buffering without wavelength ratioing. *Biophys J* 78(5):2655–2667.
7. Yasuda R, et al. (2004) Imaging calcium concentration dynamics in small neuronal compartments. *Sci STKE* 2004(219):pl5.
8. DiGregorio DA, Vergara JL (1997) Localized detection of action potential-induced presynaptic calcium transients at a Xenopus neuromuscular junction. *J Physiol* 505(Pt 3):585–592.

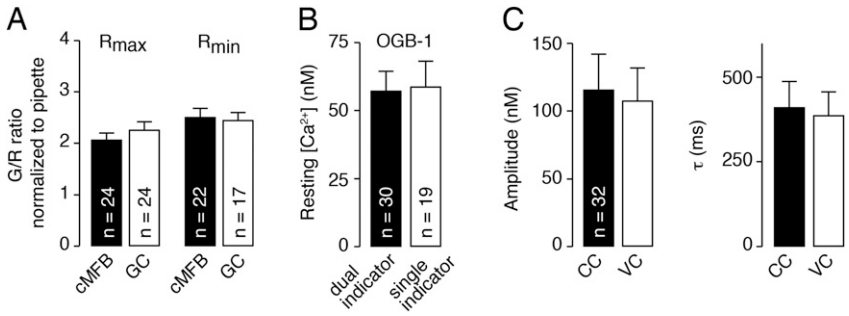

Fig. S1. Quantification of two-photon Ca^{2+} signals. (*A*) Green-over-red fluorescence ratio (G/R) determined in situ was consistently higher than in pipettes. This difference was observed for maximum (R_{max}, measured with 10 mM $CaCl_2$) and minimum (R_{min}, measured with 10 mM EGTA) fluorescence ratios. Fluorescence ratios were similar in granule cells (GC) and cMFBs ($P = 0.34$ and $P = 0.80$ for R_{max} and R_{min}, respectively; unpaired *t* test). (*B*) The overall [Ca^{2+}] at rest was 57.4 ± 7.1 nM ($n = 30$ boutons, OGB-1). Calculation with an independent single-indicator method (1) gave similar results (58.9 ± 9.3 nM, $n = 19$; $P = 0.90$; unpaired *t* test). (*C*) Action potentials in cMFBs were generally evoked by tonic current injection in current-clamp (CC) mode (*Materials and Methods*). For 300-Hz train stimulations, we used brief depolarizations to 0 mV (duration, 200 μs) in voltage-clamp (VC) mode. Ca^{2+} transients evoked by current injections and depolarizations had comparable amplitudes and decay time constants ($P = 0.35$ and $P = 0.31$, respectively; paired *t* tests).

1. Maravall M, Mainen ZF, Sabatini BL, Svoboda K (2000) Estimating intracellular calcium concentrations and buffering without wavelength ratioing. *Biophys J* 78(5):2655–2667.

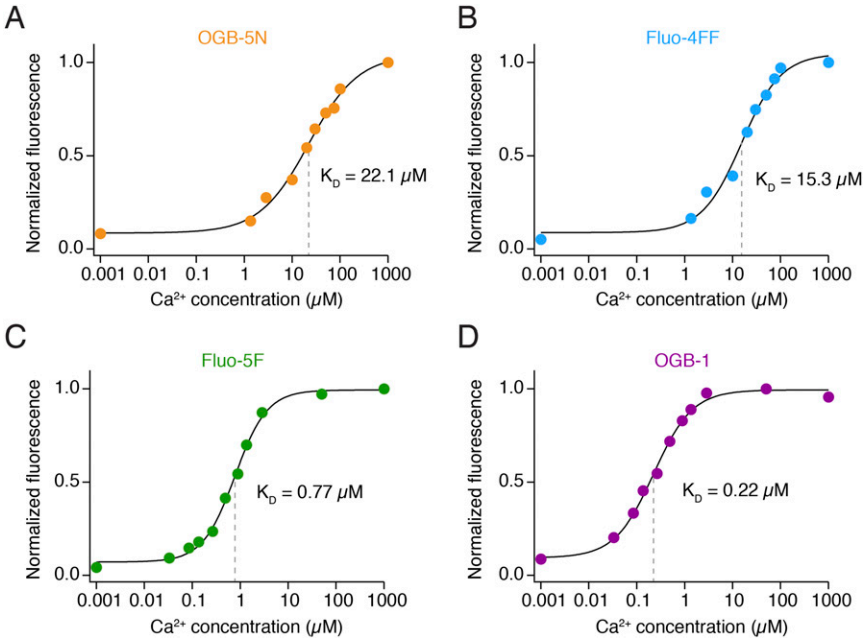

Fig. S2. Measurements of dissociation constants for Ca^{2+} indicators. (*A*–*D*) Dissociation constants (K_D) were determined in cuvettes at room temperature for the four different Ca^{2+} indicators used in the present study (OGB-5N, Fluo-4FF, Fluo-5F, and OGB-1). Green over red fluorescence ratios were measured with buffered solutions ranging from 0 to 1 mM free [Ca^{2+}]. Data were normalized to the maximum fluorescence ratio and fit with a sigmoid function (black lines). Note the logarithmic scale of the abscissa. The half-points of the functions (dashed gray lines) give the K_D of the Ca^{2+} indicators. The measured K_D values were used to scale the assumed K_D values from the literature (*SI Materials and Methods*).

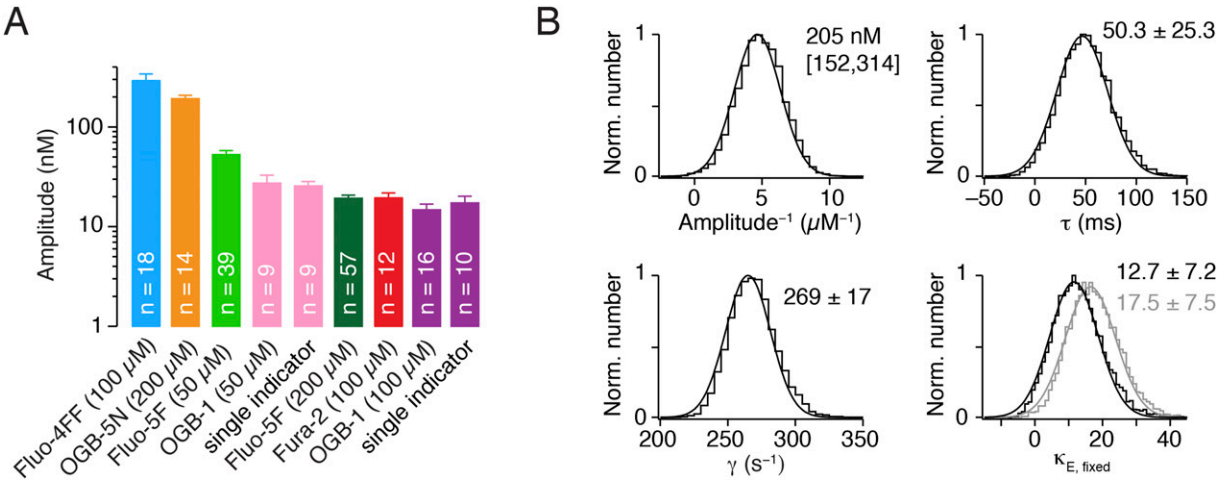

Fig. S3. Action potential-evoked amplitudes and bootstrap analysis. (*A*) Amplitude of Ca^{2+} transients recorded with different indicators. For OGB-1, amplitudes estimated by dual-indicator (1) and single-indicator (2) approaches were also compared. Note the logarithmic scale of the ordinate. (*B*) Statistical reliability of the extrapolation in Fig. 2 *C* and *D* was addressed with bootstrap analysis (3) (*Materials and Methods*). Shown are histograms of bootstrap samples for the parameters amplitude (A), decay time constant (τ), Ca^{2+}-extrusion rate (γ), and Ca^{2+}-binding ratio (κ_E). Analysis of κ_E was performed with A^{-1} (black) and τ (gray) data.

1. Maravall M, Mainen ZF, Sabatini BL, Svoboda K (2000) Estimating intracellular calcium concentrations and buffering without wavelength ratioing. *Biophys J* 78(5):2655–2667.
2. Yasuda R, et al. (2004) Imaging calcium concentration dynamics in small neuronal compartments. *Sci STKE* 2004(219):pl5.
3. Aponte Y, Bischofberger J, Jonas P (2008) Efficient Ca^{2+} buffering in fast-spiking basket cells of rat hippocampus. *J Physiol* 586(8):2061–2075.

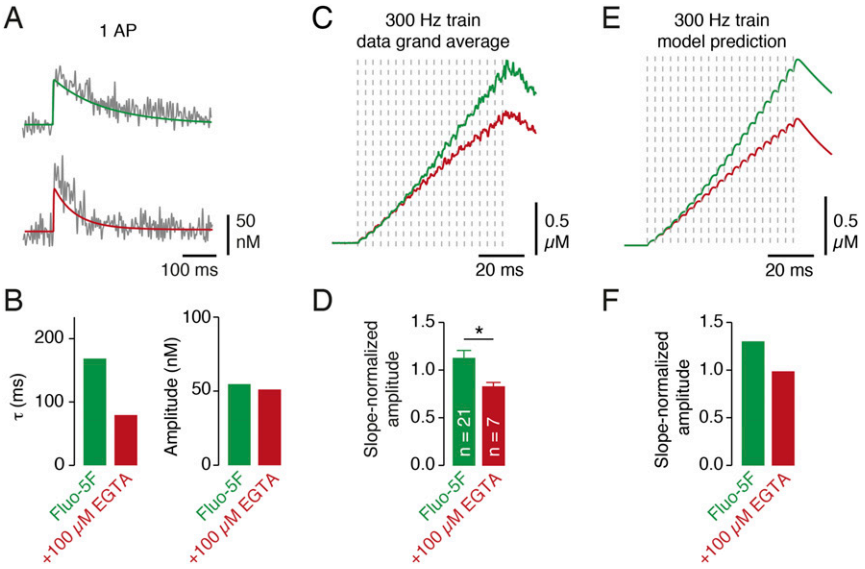

Fig. S4. Endogenous mobile Ca^{2+} buffers impact on residual Ca^{2+} transients in cMFBs. (*A*) Overlay of the Ca^{2+} transient model prediction and experimental data for a single AP with 50 μM Fluo-5F (*Upper*, green) and in addition 100 μM of the Ca^{2+} chelator EGTA (*Lower*, red). Experimental data (gray) are taken from Fig. 4*A*. (*B*) Decay time constants (τ) and amplitudes of residual Ca^{2+} transients in the simulations. The prediction matches the experimental data well (Fig. 4*B*). (*C*) Grand average of Ca^{2+} transients in response to a 300-Hz AP train (20 stimuli) in control (50 μM Fluo-5F; $n = 17$) and EGTA condition (50 μM Fluo-5F + 100 μM EGTA, $n = 7$). Data were recorded at 3-kHz sampling rate; dashed lines indicate time of APs. (*D*) Average normalized amplitude of the residual Ca^{2+} transient in response to 20 APs at 300 Hz (the amplitude was normalized to the amplitude extrapolated from the initial slope). Adding 100 μM EGTA reduced the peak amplitude by 30% ($P = 0.046$; unpaired *t* test). (*E*) Simulation of a 300-Hz train of APs (20 stimuli). Dashed lines indicate time points of APs. The amplitude of the resulting residual Ca^{2+} transient is reduced by adding 100 μM EGTA (red). (*F*) The model predicts an ~30% reduction of the residual Ca^{2+} amplitude for a 300-Hz train, corroborating our experimental observations.

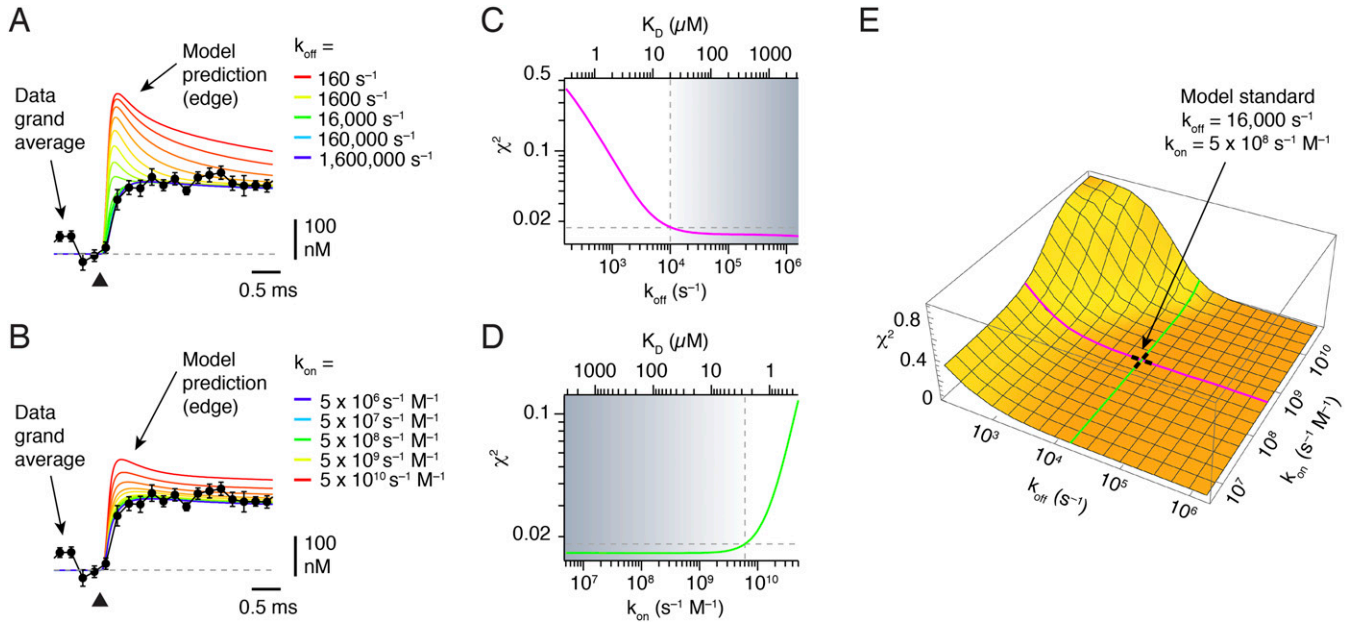

Fig. S5. Kinetics of endogenous fixed Ca^{2+} buffers. We analyzed the detailed kinetics of $[Ca^{2+}]$ rise at the edge of cMFBs. In simulations, we varied the backward (k_{off}) or forward binding-rates (k_{on}) of the endogenous fixed buffer while adjusting its total concentration such that $\kappa_{E,fixed}$ was constant. When k_{off} was low, the initial increase in $[Ca^{2+}]$ had a clear overshoot (*A*), which was not present in the experimental data. Data are from Fig. 8*E*: grand average from the edge of cMFBs ($n = 20$; bin size, 0.2 ms; error bars represent SEM). The model prediction also deviated largely from the data when k_{on} was large (*B*). (*C*) Plot of χ^2 vs. k_{off}. k_{on} was kept constant at $5 \times 10^8\ s^{-1} \cdot M^{-1}$. Top axis denotes the K_D of the endogenous buffer. (*D*) Plot of χ^2 vs. k_{on}. k_{off} was kept constant at 16,000 s^{-1}. Top axis denotes the K_D of the endogenous buffer. (*E*) Plot of χ^2 vs. k_{on} and k_{off}. The model standard combination is indicated (black cross). We thus infer that k_{off} must be larger than 10,000 s^{-1}, and $k_{on} < 6 \times 10^9\ ms^{-1} \cdot \mu M^{-1}$, with K_D of the endogenous buffers >20 μM. Our boundaries for k_{off} and K_D are similar to previous approximations obtained at the calyx of Held presynaptic terminal (1, 2) and indicate that the endogenous fixed buffers at cMFBs are of low affinity with very fast kinetics.

1. Habets RL, Borst JG (2006) An increase in calcium influx contributes to post-tetanic potentiation at the rat calyx of Held synapse. *J Neurophysiol* 96(6):2868–2876.
2. Nakamura Y, et al. (2015) Nanoscale distribution of presynaptic Ca^{2+} channels and its impact on vesicular release during development. *Neuron* 85(1):145–158.

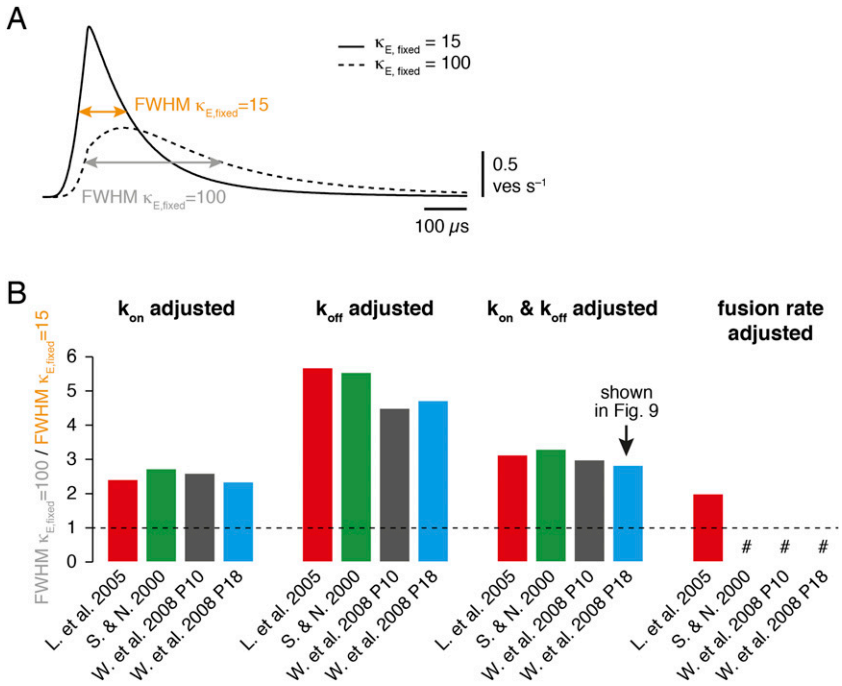

Fig. S6. Simulations with different release schemes. When comparing the time course of the vesicular release rate with low ($\kappa_{E,fixed}$ = 15) and high ($\kappa_{E,fixed}$ = 100) Ca^{2+}-binding ratio of the fixed endogenous buffers, the full-width at half-maximum (FWHM) was smaller for $\kappa_{E,fixed}$ = 15 (Fig. 9). We tested the robustness of this finding by varying the release scheme used in the simulations and by varying the required adjustments to obtain a vesicular release probability of 0.3. (*A*) Time course of the release rate for a single AP differs for low and high $\kappa_{E,fixed}$. The FWHM is illustrated. (*B*) The ratio of FWHM between $\kappa_{E,fixed}$ = 100 and $\kappa_{E,fixed}$ = 15 is plotted for the various conditions. The four different release schemes are color-coded [Lou et al. (1); Schneggenburger and Neher (2); and Wang et al. (3), for P9–11 and P16–19]. To adapt the release schemes to our preparation and recording conditions, we first adjusted all rates to 37 °C, assuming a Q_{10} factor of 3. Second, the following four strategies were compared with obtain a vesicular release probability of 0.3 (4): increasing k_{on}, decreasing k_{off}, increasing k_{on}, and decreasing k_{off} with the same factor or increasing the fusion rate. In some cases it was impossible to achieve a release probability of 0.3 with physically plausible values (#). With all tested release schemes, the FWHM of the release rate was more than twofold longer for $\kappa_{E,fixed}$ = 100 compared with $\kappa_{E,fixed}$ = 15. The resulting parameters used for the simulations depicted in Fig. 9*B* (modified Wang et al. P16–19 scheme) were as follows: k_{on} = 135 $s^{-1}{\cdot}M^{-1}$, k_{off} = 14,742 s^{-1}, vesicle fusion rate (γ) = 6,000 s^{-1}, and b = 0.25. We also repeated these simulations with a distance between vesicle and nearest Ca^{2+} channel of 50 nm instead of 20 nm, which prolonged the release rate FWHM from 114 to 356 μs (using Wang et al. P16–19 scheme and $\kappa_{E,fixed}$ = 15). However, the prolongation of the release rate with $\kappa_{E,fixed}$ = 100 was similar for all tested release schemes (i.e., greater than twofold). Thus, our findings are independent of the implementation of the release scheme and the vesicle to Ca^{2+} channel coupling distance.

1. Lou X, Scheuss V, Schneggenburger R (2005) Allosteric modulation of the presynaptic Ca^{2+} sensor for vesicle fusion. *Nature* 435(7041):497–501.
2. Schneggenburger R, Neher E (2000) Intracellular calcium dependence of transmitter release rates at a fast central synapse. *Nature* 406(6798):889–893.
3. Wang LY, Neher E, Taschenberger H (2008) Synaptic vesicles in mature calyx of Held synapses sense higher nanodomain calcium concentrations during action potential-evoked glutamate release. *J Neurosci* 28(53):14450–14458.
4. Hallermann S, et al. (2010) Bassoon speeds vesicle reloading at a central excitatory synapse. *Neuron* 68(4):710–723.

Table S1. Model parameters used in simulations

Parameter (units)	Concentration (μM)	K_D (μM)	k_{on} ($s^{-1}\cdot M^{-1}$)	k_{off} (s^{-1})	D ($\mu m^2\cdot s^{-1}$)	κ
Ca^{2+}					220[a]	
$[Ca^{2+}]_{rest}$	0.057[b]					
Endogenous buffers						
Fixed	480[c]	32[d]	5×10^{8}[d]	16,000[d]	0	15[e]
Mobile	100[f]	0.2[g]	0.05×10^{8}[g]	1[g]	20[h]	500[ii]
ATP	370[j]	200[k]	5×10^{8}[k]	100,000[k]	220[k]	1.8[l]
Gluconate	150,000	57,000[m]	1×10^{8}[m]	5,700,000[m]	220	2.6[m]
Ca^{+} indicators						
OGB-1	50	0.24[n]	4.3×10^{8}[o]	103[p]	140	129[q]
	100					269[q]
OGB-5N	200	24[n]	2.5×10^{8}[r]	6,000[p]	140	8.2[q]
Fluo-5F	50	0.83[n]	3×10^{8}[o]	249[p]	140	50[q]
	200					208[q]
Fluo-4FF	100	16.6[n]	3×10^{8}[o]	4.98[p]	140	5.9[q]

Concentration, dissociation constants (K_D), binding kinetics (k_{on} and k_{off}), diffusion coefficients (D), and Ca^{2+}-binding ratios (κ) used in simulations.

[a]Ref. 1.

[b]Compare with Fig. S1*B*.

[c]Calculated as $K_D \times \kappa$.

[d]Refs. 2 and 3; compare with Fig. S5.

[e]Compare with Fig. 2.

[f]Compare with Fig. 4.

[g]Based on Fig. 4, the kinetic parameters of the mobile buffer were set to values of EGTA at physiological temperature and pH 7.3 (4).

[h]Ref. 5.

[i]Calculated as concentration/K_D. Note that the Ca^{2+}-binding ratio of the mobile buffer is misleading, because kinetics of extrusion and equilibration with the mobile buffer are comparable at cMFBs (6) (*Discussion*).

[j]Calculated free ATP concentration.

[k]Ref. 7.

[l]Calculated as concentration/K_D.

[m]Ref. 8.

[n]Based on Fig. S2; see *SI Materials and Methods*.

[o]Ref. 9.

[p]Calculated as $K_D \times k_{on}$.

[q]Incremental Ca^{2+}-binding ratio (Eq. **5**).

[r]Ref. 10.

1. Allbritton NL, Meyer T, Stryer L (1992) Range of messenger action of calcium ion and inositol 1,4,5-trisphosphate. *Science* 258(5089):1812–1815.
2. Habets RL, Borst JG (2006) An increase in calcium influx contributes to post-tetanic potentiation at the rat calyx of Held synapse. *J Neurophysiol* 96(6):2868–2876.
3. Klingauf J, Neher E (1997) Modeling buffered Ca^{2+} diffusion near the membrane: Implications for secretion in neuroendocrine cells. *Biophys J* 72(2 Pt 1):674–690.
4. Smith PD, Liesegang GW, Berger RL, Czerlinski G, Podolsky RJ (1984) A stopped-flow investigation of calcium ion binding by ethylene glycol bis(beta-aminoethyl ether)-N,N′-tetraacetic acid. *Anal Biochem* 143(1):188–195.
5. Schmidt H, Brown EB, Schwaller B, Eilers J (2003) Diffusional mobility of parvalbumin in spiny dendrites of cerebellar Purkinje neurons quantified by fluorescence recovery after photobleaching. *Biophys J* 84(4):2599–2608.
6. Lee SH, Schwaller B, Neher E (2000) Kinetics of Ca^{2+} binding to parvalbumin in bovine chromaffin cells: Implications for $[Ca^{2+}]$ transients of neuronal dendrites. *J Physiol* 525(Pt 2): 419–432.
7. Meinrenken CJ, Borst JGG, Sakmann B (2002) Calcium secretion coupling at calyx of Held governed by nonuniform channel-vesicle topography. *J Neurosci* 22(5):1648–1667.
8. Woehler A, Lin KH, Neher E (2014) Calcium-buffering effects of gluconate and nucleotides, as determined by a novel fluorimetric titration method. *J Physiol* 592(Pt 22):4863–4875.
9. Yasuda R, et al. (2004) Imaging calcium concentration dynamics in small neuronal compartments. *Sci STKE* 2004(219):pl5.
10. DiGregorio DA, Vergara JL (1997) Localized detection of action potential-induced presynaptic calcium transients at a Xenopus neuromuscular junction. *J Physiol* 505(Pt 3):585–592.